INSTITUTE OF PHYSICS PUBLISHING SMART MATERIALS AND STRUCTURES
Smart Mater. Struct. **13** (2004) 175–183 PII: S0964-1726(04)72388-5

Static responses of a multilayered anisotropic piezoelectric structure to point force and point charge*

B Yang[1,3], E Pan[2] and V K Tewary[1]

[1] Materials Reliability Division, National Institute of Standards and Technology, Boulder, CO 80305, USA
[2] Department of Civil Engineering, University of Akron, Akron, OH 44325, USA

E-mail: boyang@fit.edu

Received 28 April 2003, in final form 20 November 2003
Published 15 December 2003
Online at stacks.iop.org/SMS/13/175 (DOI: 10.1088/0964-1726/13/1/020)

Abstract
This paper studies three-dimensional (3D) static responses of a multilayered anisotropic piezoelectric structure due to a point force and point charge. The materials in each layer are homogeneous, generally anisotropic, and linearly piezoelectric, and in general different from one another. The interfaces between adjacent layers are perfectly bonded. The generalized Stroh formalism and two-dimensional (2D) Fourier transforms are employed to find the responses in terms of a 2D integral. For a layered structure made of ten alternating layers of piezoelectric AlN and InN on an InN substrate, we show that the responses due to the point force and point charge are greatly influenced by the material layering, showing complicated patterns through the layer thickness. Furthermore, the responses exhibit the asymptotic behavior in the case of homogeneous infinite space/half-space in a very short distance to the point source, about one tenth of the layer thickness. The complicated responses due to the layered heterogeneity dictate the need for a general 3D analysis in the design of such smart structures.

1. Introduction

Owing to their special feature of transforming energy between electric and mechanical types, piezoelectric materials are ideal for use in transducers, sensors, and actuators (see, e.g., Tzou 1993, Yang and Tiersten 1997). To assist in the design of these components, various numerical methods have been applied to the modeling of piezoelectric structures, including the finite-difference method, the finite-element method, and the boundary-element (BE) method. While the first two methods require discretization of the problem domain, the BE method needs discretization of the problem boundary only. However, the most efficient use of the BE formulation requires the fundamental solutions of the associated system (Denda and Lua 1999, Liu and Fan 2001, Davi and Milazzo 2002). The associated fundamental solution can also be directly used to analytically solve the special case of inclusions. Identifying such fundamental solutions could be difficult if the problem domain is complex.

Under the assumption of two-dimensional (2D) deformation, the line-source fundamental solutions (i.e., elastic displacement and electric potential) and various inclusion problems of anisotropic piezoelectricity have been solved. These include problems in an infinite plane, half-plane, and bimaterial plane (Barnett and Lothe 1975, Chung and Ting 1996, Pan 1999, Ru 2000, 2001). Fundamental solutions for anisotropic piezoelectricity under three-dimensional (3D) deformation are much more complicated than those under 2D deformation. By assuming transverse isotropy of piezoelectricity, the point-force and point-charge solutions in an infinite space, half-space, and bimaterial space have been derived by using the potential-function method (see, e.g., Dunn and Wienecke 1996, 1999, Ding *et al* 1997, 1999).

* Publication of the National Institute of Standards and Technology, an agency of the US Govt; not subject to copyright.
[3] Author to whom any correspondence should be addressed. Current address: Department of Mechanical and Aerospace Engineering, Florida Tech, Melbourne, FL 32901, USA.

Finding the 3D responses in a generally anisotropic piezoelectric infinite space has been a great challenge. Previously, the solutions were expressed in terms of a numerical integral (see, e.g., Deeg 1980, Chen 1993). Recently, however, Akamatsu and Tanuma (1997) derived an explicit expression without a numerical integral using the extended Stroh formalism. Pan and Tonon (2000) derived another explicit expression without a numerical integral using the Radon transform and the residue theorem. They also presented the derivatives of the elastic displacement and electric potential with respect to coordinates of the field point. These derivatives lead to the elastic strain and hence stress and electric field, which are required in the BE method. An even more complicated problem is to derive fundamental solutions in anisotropic piezoelectric half-spaces and bimaterials. Using the Fourier-transform method, extended Stroh formalism (Barnett and Lothe 1975, Ting 1996), and Mindlin's superposition method, Pan and Yuan (2000) and Pan (2001, 2002) have recently developed these fundamental solutions, which involve only a line integral in a finite interval.

In this paper, we apply the extended Stroh formalism and 2D Fourier transforms to derive the 3D fundamental response in a multilayered anisotropic piezoelectric structure. The boundary-value problem of the multilayered piezoelectric structure subjected to a point force and a point charge is transformed in the Fourier domain, and solved analytically. The materials in each layer are homogeneous, generally anisotropic, linearly piezoelectric, and in general different from one another. The interfaces are perfectly bonded. General boundary conditions that ensure unique solutions are applied to the top and bottom surfaces of the structure. We examine a structure made of ten alternating layers of piezoelectric AlN/InN over an InN substrate. Our numerical results show that, in a structure with surfaces and interfaces, the Green responses exhibit asymptotic behavior in the case of homogeneous infinite space/half-space in a very short distance from the point source, about one tenth of the layer thickness. A general 3D analysis is, in general, required in the design of such smart structures.

2. Formulation

We consider a layered plate that consists of n layers of different homogeneous and linearly anisotropic piezoelectric materials, as shown in figure 1. A Cartesian coordinate system (x_1, x_2, x_3) is attached to the plate in such a way that the x_1–x_2 plane lies on the top surface and the plate occupies $x_3 \geqslant 0$. Each layer occupies the region $h_{j-1} \leqslant x_3 \leqslant h_j$ $(j = 1, 2, \ldots, n)$, with $0 = h_0 < h_1 < \cdots < h_n$. If $h_n = \infty$ the layered plate becomes a layered half-space. The boundary conditions at $x_3 = h_0$ and h_n and interfacial continuity conditions at $x_3 = h_j$ $(j = 1, 2, \ldots, n-1)$ that are needed to ensure unique solutions will be described later.

The equations of the mechanical and electric equilibriums for each layer of the plate are given by (Barnett and Lothe 1975, Pan 1999)

$$\sigma_{ji,j} + f_i = 0, \qquad D_{i,i} - q = 0, \tag{1}$$

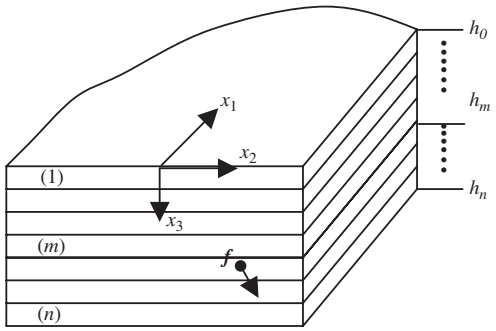

Figure 1. An n-layered piezoelectric plate.

where σ_{ji} is the stress component, D_i is the electric displacement component, f_i is the body force component, and q is the electric charge. The comma in the subscript indicates partial differentiation with respect to the coordinate that follows. The repeated subscript implies conventional Einstein summation over its range.

The constitutive laws for each homogeneous layer are given by

$$\sigma_{ji} = C_{jilm}\gamma_{lm} - e_{kji}E_k, \qquad D_i = e_{ijk}\gamma_{jk} + \varepsilon_{ij}E_j, \tag{2}$$

where γ_{lm} is the infinitesimal strain component, E_k is the electric field component, and C_{jilm}, e_{kji}, and ε_{ij} are, respectively, the elastic stiffness, piezoelectric coefficient, and dielectric constant. The strain and electric field are respectively related to the elastic displacement $\boldsymbol{u}$ and electric potential ϕ by

$$\gamma_{ij} = \tfrac{1}{2}(u_{i,j} + u_{j,i}), \qquad E_i = -\phi_{,i}. \tag{3}$$

For convenience in analyzing the anisotropic piezoelectric problem, the notation of Barnett and Lothe (1975) is adopted in the present work. This notation introduces the extended displacement, strain, stress, and materials constants as follows:

$$u_I = \begin{cases} u_i & I\ (=i) = 1, 2, 3, \\ \phi & I = 4, \end{cases} \tag{4}$$

$$\gamma_{Ij} = \begin{cases} \gamma_{ij} & I\ (=i) = 1, 2, 3, \\ -E_j & I = 4, \end{cases} \tag{5}$$

$$\sigma_{iJ} = \begin{cases} \sigma_{ij} & J\ (=j) = 1, 2, 3, \\ D_i & J = 4, \end{cases} \tag{6}$$

$$C_{iJKl} = \begin{cases} C_{ijkl} & J\ (=j), \quad K\ (=k) = 1, 2, 3, \\ e_{lij} & J\ (=j) = 1, 2, 3, \quad K = 4, \\ e_{ikl} & J = 4, \quad K\ (=k) = 1, 2, 3, \\ -\varepsilon_{il} & J = K = 4, \end{cases} \tag{7}$$

where the upper-case subscripts range from 1 to 4, and the lower-case subscripts from 1 to 3.

In terms of this shorthand notation, the equilibrium equations in equation (1) can be unified as

$$\sigma_{jI,j} + f_I = 0, \tag{8}$$

with

$$f_I = \begin{cases} f_i & I\ (=i) = 1, 2, 3, \\ -q & I = 4. \end{cases} \tag{9}$$

Similarly, the constitutive laws in equation (2) are recast as

$$\sigma_{iJ} = C_{iJKl}\gamma_{Kl}. \tag{10}$$

In the following, the general solution of piezoelectricity within the framework of generalized Stroh formalism and 2D Fourier transformation (Ting 1996, Pan and Yuan 2000) is first summarized. Then, the problem of multilayered piezoelectric structure formulated above is solved by enforcing boundary and interfacial conditions. Appropriate special solutions are employed to expedite the numerical evaluation of the physical quantities.

2.1. General solution in Stroh formalism

We apply the following 2D Fourier transform (y_1, y_2) to the in-plane variables of a field quantity, for instance, u_I, as

$$\tilde{u}_I(y_1, y_2, x_3) = \int\int u_I(x_1, x_2, x_3)\mathrm{e}^{\mathrm{i}y_\alpha x_\alpha}\,\mathrm{d}x_1\,\mathrm{d}x_2, \tag{11}$$

where e stands for the *exponential* function, i denotes the unit of imaginary number, $\sqrt{-1}$, and the Greek subscript takes values 1 and 2. The integral limits are $(-\infty, \infty)$ along both coordinates x_1 and x_2. Thus, in the Fourier-transformed domain, the governing equation (8), in terms of the extended displacement (after applying the constitutive laws, equation (10)), becomes

$$\begin{aligned} &C_{3IK3}\tilde{u}_{K,33} - \mathrm{i}(C_{\alpha IK3} + C_{3IK\alpha})y_\alpha\tilde{u}_{K,3} - C_{\alpha IK\beta}y_\alpha y_\beta\tilde{u}_K \\ &\quad = -f_I\mathrm{e}^{\mathrm{i}x^0_\alpha y_\alpha}\delta(x_3 - x^0_3), \end{aligned} \tag{12}$$

where the body force term in equation (8) is replaced by a concentrated force $f_I\delta(\boldsymbol{x} - \boldsymbol{x}^0)$ applied at point $\boldsymbol{x}^0$, where $\delta(\boldsymbol{x} - \boldsymbol{x}^0)$ is the Dirac delta function.

Solving the above ordinary differential equation yields a general solution of the extended displacement in the transformed domain (Ting 1996):

$$\tilde{\boldsymbol{u}}(y_1, y_2, x_3) = \boldsymbol{a}\mathrm{e}^{-\mathrm{i}p\eta x_3}, \tag{13}$$

where η is the norm of (y_1, y_2), and p and $\mathbf{a}$ are eigenvalue and eigenvector of the Stroh's eigenequation. Taking the derivative of equation (13) and applying the constitutive law, equation (10), results in the solution of the extended stress in the transformed domain,

$$\tilde{\boldsymbol{t}} = -\mathrm{i}\eta\boldsymbol{b}\mathrm{e}^{-\mathrm{i}p\eta x_3}, \qquad \tilde{\boldsymbol{s}} = -\mathrm{i}\eta\boldsymbol{c}\mathrm{e}^{-\mathrm{i}p\eta x_3}, \tag{14}$$

where $\boldsymbol{t} \equiv (\sigma_{13}, \sigma_{23}, \sigma_{33}, D_3)^{\mathrm{T}}$ and $\boldsymbol{s} \equiv (\sigma_{11}, \sigma_{12}, \sigma_{22}, D_1, D_2)^{\mathrm{T}}$ respectively consist of the out-of-plane and in-plane stress and electric displacement components, and $\boldsymbol{b}$ and $\boldsymbol{c}$ are the eigenvectors corresponding to the vectors $\boldsymbol{t}$ and $\boldsymbol{s}$, respectively, and related to $\boldsymbol{a}$ and p.

There exist eight sets of eigenvalue p_I and the associated eigenvectors $\boldsymbol{a}_I, \boldsymbol{b}_I$, and $\boldsymbol{c}_I$. They are arranged in the following way:

$$\begin{aligned} &\mathrm{Im}\,p_I > 0, \qquad p_{I+4} = \bar{p}_I, \qquad \boldsymbol{a}_{I+4} = \bar{\boldsymbol{a}}_I, \\ &\boldsymbol{b}_{I+4} = \bar{\boldsymbol{b}}_I, \qquad \boldsymbol{c}_{I+4} = \bar{\boldsymbol{c}}_I \qquad (I = 1, 2, 3, 4), \\ &\boldsymbol{A} = [\boldsymbol{a}_1, \boldsymbol{a}_2, \boldsymbol{a}_3, \boldsymbol{a}_4], \qquad \boldsymbol{B} = [\boldsymbol{b}_1, \boldsymbol{b}_2, \boldsymbol{b}_3, \boldsymbol{b}_4], \\ &\boldsymbol{C} = [\boldsymbol{c}_1, \boldsymbol{c}_2, \boldsymbol{c}_3, \boldsymbol{c}_4], \end{aligned} \tag{15}$$

where Im stands for the imaginary part and the overbar denotes the complex conjugate. Assuming that p_I $(I = 1, 2, 3, 4)$ are distinct, the general solutions are obtained by superposing the eight solutions of equations (13) and (14), as

$$\tilde{\boldsymbol{u}} = \mathrm{i}\eta^{-1}\bar{\boldsymbol{A}}\langle\mathrm{e}^{-\mathrm{i}\bar{p}\eta x_3}\rangle\boldsymbol{v} + \mathrm{i}\eta^{-1}\boldsymbol{A}\langle\mathrm{e}^{-\mathrm{i}p\eta x_3}\rangle\boldsymbol{w}, \tag{16}$$

$$\begin{aligned} \tilde{\boldsymbol{t}} &= \bar{\boldsymbol{B}}\langle\mathrm{e}^{-\mathrm{i}\bar{p}\eta x_3}\rangle\boldsymbol{v} + \boldsymbol{B}\langle\mathrm{e}^{-\mathrm{i}p\eta x_3}\rangle\boldsymbol{w}, \\ \tilde{\boldsymbol{s}} &= \bar{\boldsymbol{C}}\langle\mathrm{e}^{-\mathrm{i}\bar{p}\eta x_3}\rangle\boldsymbol{v} + \boldsymbol{C}\langle\mathrm{e}^{-\mathrm{i}p\eta x_3}\rangle\boldsymbol{w} \end{aligned} \tag{17}$$

where $\boldsymbol{v}(y_1, y_2)$ and $\boldsymbol{w}(y_1, y_2)$ are unknown complex vectors and

$$\langle\mathrm{e}^{-\mathrm{i}p\eta x_3}\rangle = \mathrm{diag}[\mathrm{e}^{-\mathrm{i}p_1\eta x_3}, \mathrm{e}^{-\mathrm{i}p_2\eta x_3}, \mathrm{e}^{-\mathrm{i}p_3\eta x_3}, \mathrm{e}^{-\mathrm{i}p_4\eta x_3}]. \tag{18}$$

Note that the above matrix $\boldsymbol{C}$ with 5×4 elements is different from the fourth-order elastic stiffness tensor C_{ijkl} or the extended stiffness tensor C_{iJKl}.

2.2. Fundamental solution for multilayered plate

Let us apply a concentrated (extended) force f_I at an arbitrary point (x^0_1, x^0_2, d). Utilizing the general solution developed in the previous subsection, the total solution due to the concentrated force f_I in the layered plate (figure 1) can be written in the following form:

$$\begin{aligned} \tilde{\boldsymbol{u}}_m(y_1, y_2, x_3)\mathrm{e}^{-\mathrm{i}y_\alpha x^0_\alpha} &= \tilde{\boldsymbol{u}}^{(s)}_m(y_1, y_2, x_3) \\ &+ \mathrm{i}\eta^{-1}\bar{\boldsymbol{A}}_m\langle\mathrm{e}^{-\mathrm{i}\bar{p}_m\eta(x_3 - h_{m-1})}\rangle\boldsymbol{v}_m \\ &+ \mathrm{i}\eta^{-1}\boldsymbol{A}_m\langle\mathrm{e}^{-\mathrm{i}p_m\eta(x_3 - h_m)}\rangle\boldsymbol{w}_m, \end{aligned} \tag{19}$$

$$\begin{aligned} \tilde{\boldsymbol{t}}_m(y_1, y_2, x_3)\mathrm{e}^{-\mathrm{i}y_\alpha x^0_\alpha} &= \tilde{\boldsymbol{t}}^{(s)}_m(y_1, y_2, x_3) \\ &+ \bar{\boldsymbol{B}}_m\langle\mathrm{e}^{-\mathrm{i}\bar{p}_m\eta(x_3 - h_{m-1})}\rangle\boldsymbol{v}_m + \boldsymbol{B}_m\langle\mathrm{e}^{-\mathrm{i}p_m\eta(x_3 - h_m)}\rangle\boldsymbol{w}_m, \end{aligned} \tag{20a}$$

$$\begin{aligned} \tilde{\boldsymbol{s}}_m(y_1, y_2, x_3)\mathrm{e}^{-\mathrm{i}y_\alpha x^0_\alpha} &= \tilde{\boldsymbol{s}}^{(s)}_m(y_1, y_2, x_3) \\ &+ \bar{\boldsymbol{C}}_m\langle\mathrm{e}^{-\mathrm{i}\bar{p}_m\eta(x_3 - h_{m-1})}\rangle\boldsymbol{v}_m + \boldsymbol{C}_m\langle\mathrm{e}^{-\mathrm{i}p_m\eta(x_3 - h_m)}\rangle\boldsymbol{w}_m, \end{aligned} \tag{20b}$$

for $m = 1, 2, \ldots, n$, where the subscript m denotes the mth layer, and $\boldsymbol{v}_m$ and $\boldsymbol{w}_m$ are unknown vectors to be determined from (given) interfacial and boundary conditions. In addition, $\tilde{\boldsymbol{u}}^{(s)}_m$, $\tilde{\boldsymbol{t}}^{(s)}_m$, and $\tilde{\boldsymbol{s}}^{(s)}_m$ are special solutions. The special solutions should be chosen according to the location of the applied force $\boldsymbol{f}$ such that the general-part solutions, i.e., unknown tensors $\boldsymbol{v}_m$ and $\boldsymbol{w}_m$, are nonsingular in the physical space and can be evaluated efficiently.

Four different locations of $\boldsymbol{f}$ may arise: on the top surface $(d = h_0 = 0)$, in the kth layer $(h_{k-1} < d < h_k)$, on the kth interface $(d = h_k)$, and on the bottom surface $(h = h_n)$. In the first case, $d = h_0 = 0$, the special solutions are taken to be the surface solution in the case of a half-space (Pan 2002) in the first layer, and to be zero in the other layers. In the second case, $h_{k-1} < d < h_k$, the special solutions are taken to be the fundamental solutions of an infinite space in the kth layer where $\boldsymbol{f}$ is applied, and to be zero in the other layers. The physical counterparts of the infinite-space fundamental solutions can be evaluated analytically (Akamatsu and Tanuma 1997, Pan and Tonon 2000). In the third case, $d = h_{k-1}$, the special solutions are assigned to be the interfacial fundamental solutions of the bimaterials (Pan and Yuan 2000) in the $(k-1)$th and kth layers which share the interface. In the other layers, they are equal to zero. In the last case, $d = h_n$, which is similar to the first case, the surface response of an upper half-space is taken to

substitute for the special solution in the nth layer. Otherwise, it is equal to zero. The physical counterparts of the bimaterial and half-space solutions can be efficiently evaluated involving only a one-dimensional integral over a finite interval (Pan and Yuan 2000, Pan 2002).

Now, we impose a proportional spring-type boundary condition along the top and bottom surfaces,

$$\begin{aligned} \boldsymbol{I}_1\boldsymbol{u}_1 + \boldsymbol{J}_1\boldsymbol{t}_1 = 0 \qquad & \text{at } x_3 = 0, \\ \boldsymbol{I}_n\boldsymbol{u}_n + \boldsymbol{J}_n\boldsymbol{t}_n = 0 \qquad & \text{at } x_3 = h_n, \end{aligned} \tag{21}$$

where $\boldsymbol{I}_1$, $\boldsymbol{J}_1$, $\boldsymbol{I}_n$, and $\boldsymbol{J}_n$ are given constant matrices. Across the interfaces, the extended displacement and traction vectors are assumed to be continuous,

$$\begin{gathered} \boldsymbol{u}_{m-1} = \boldsymbol{u}_m, \qquad \boldsymbol{t}_{m-1} = \boldsymbol{t}_m, \qquad \text{at } x_3 = h_m, \\ \text{for } m = 1, \ldots, n-1. \end{gathered} \tag{22}$$

Under these boundary and interfacial conditions, the unknown general-part solution, i.e., vectors $\boldsymbol{v}_m$ and $\boldsymbol{w}_m$, can be solved. Substituting equations (19) and (20*a*) into (21) and (22) yields a linear system of algebraic equations,

$$\boldsymbol{E}\boldsymbol{q} = \boldsymbol{\beta}, \tag{23}$$

where $\boldsymbol{q}$ $(\equiv[\boldsymbol{v}_1^{\mathrm{T}}, \boldsymbol{w}_1^{\mathrm{T}}, \ldots, \boldsymbol{v}_m^{\mathrm{T}}, \boldsymbol{w}_m^{\mathrm{T}}, \ldots, \boldsymbol{v}_n^{\mathrm{T}}, \boldsymbol{w}_n^{\mathrm{T}}]_{8n}^{\mathrm{T}})$ is an unknown vector, $\boldsymbol{\beta}$ is a constant vector of dimension $8n$, and $\boldsymbol{E}$ is the stiffness matrix of dimension $8n \times 8n$. By inverting $\boldsymbol{E}$, the unknown vectors $\boldsymbol{v}_m$ and $\boldsymbol{w}_m$ can be solved for each layer at a given point $\boldsymbol{y}$ in the Fourier-transformed domain. Substituting these solutions back into equations (19) and (20), the extended displacement and stress can then be obtained in the transformed domain.

Once the transformed-domain solution is derived, the physical responses due to an extended point force f_I are obtained by using the Fourier-inverse transform, for instance, of u_I, as

$$u_I(x_1, x_2, x_3) = \frac{1}{(2\pi)^2} \int\int \tilde{u}_I(y_1, y_2, x_3) \mathrm{e}^{-\mathrm{i}y_\alpha x_\alpha} \, \mathrm{d}y_1 \, \mathrm{d}y_2, \tag{24}$$

where the integral limits in both coordinates are from $-\infty$ to ∞.

3. Numerical results

In this section, we apply the previous formulation to examine the 3D piezoelectric fields in a multilayered piezoelectric AlN/InN structure subjected to a point force and a point charge. The layered structure consists of ten layers of alternating AlN and InN and a semi-infinite AlN substrate. The interfaces between adjacent dissimilar materials are perfectly bonded. The layers have the same thickness, h, set to be 10 nm. The thickness of the substrate is set to be $10^5 h$, which is sufficiently large that the substrate surface exercises no influence on the field of interest near the loading point. The point force is applied on the top surface to simulate an indentation test. The point charge, on the other hand, is placed in the middle plane of the second layer counted from the top to simulate a sink or a source in the layered structure. The materials constants in the reduced notation (i.e., $C_{i'j'}$—C_{ijkl} with i'—ij and j'—kl, and $e_{ij'}$—e_{ijk} with j'—jk: 1—11; 2—22; 3—33; 4—23; 5—31; 6—12) are given in table 1 (Jogai 2001). The origin of the Cartesian coordinate system is fixed at the loading point in the point-force case and vertically above the charge on the top surface in the point-charge case. The crystallographic base axes are, respectively, parallel to each of the coordinates. The above structure with an additional artificial interface at the middle plane of each layer was also examined, which virtually contains 20 layers in the numerical calculation. The numerical results were identical (within the computational accuracy—about a relative error of 0.01%) to those to be presented below. Since the different parts of the solution in equations (19) and (20*a*), (20*b*) are evaluated by completely different formulations—the infinite-space part by the analytical Radon transform and residue theorem (Pan and Tonon 2000), the half-space and interfacial parts by the numerical methods developed by Pan and Yuan (2000) and Pan (2002), and the rest by the present numerical method—the consistency of the solutions of the 10- and 20-layer structures has demonstrated the validity and accuracy of the present formulation of piezoelectric multilayers.

3.1. A point force applied on the top surface

We first examine the case of a point force at (0, 0, 0) on the top surface. The point force may be directed along any one of the three axes. Its magnitude is equal to 10^{-7} N. The top surface is, except at the location of the point force, free of traction, i.e., $t_i = (0, 0, 0)$, and is perfectly insulated, i.e., normal electric displacement $D_3 = 0$. The conditions of zero elastic displacement and zero electric potential are imposed on the remote bottom surface. These are the boundary conditions corresponding to equation (21). Also, the continuity conditions of displacement, traction, electric potential, and normal component of electric displacement across the interfaces, i.e., equation (22), are enforced. The numerical results of the point-force response under these conditions are plotted in figures 2–8 and discussed below.

The angular variations of (nonzero) components of the piezoelectric field (including displacement, stress, electric potential, and electric displacement) on the top surface around the loading point are shown in figures 2–4. The radius of the circle is $3h$. The three figures correspond to the point force acting along each of the three axes. Because this circle is on the top surface, the calculated traction and normal component of electric displacement in all these cases are equal to zero (within the computational accuracy), consistent with the imposed boundary conditions. Figures 2–4 show that the piezoelectric components are either symmetric or antisymmetric with respect to the x_1- and x_2-axes. The fields due to the point force acting along the x_1- and x_2-axis have a phase-angle difference of 90°, which coincides with the rotation angle of the two force directions. Simulations were also performed for other cases where some of the layers are rotated. If the rotation of medium is around the x_3-axis, these plots in figures 2–4 are not changed because of the transverse isotropy of the media relative to this axis. However, if the rotation of medium is around an in-plane axis, the piezoelectric fields are completely different. A detailed analysis of this effect will be given in a future article.

Table 1. Materials properties for AlN and InN in the reduced notation (elastic constant C_{ij} in 10^9 Pa, piezoelectric constants e_{ij} in C m^{-2}, and dielectric constants ε_{ij} equal to $\varepsilon_{ijr} \times 8.854 \times 10^{-12}$ C V^{-1} m^{-1}). The other nonzero components include C_{22} (=C_{11}), C_{23} (=C_{13}), C_{55} (=C_{44}), C_{66} (=(C_{11}—C_{12})/2), e_{32} (=e_{31}), e_{24} (=e_{15}), and ε_{22} (=ε_{11}).

Material	C_{11}	C_{12}	C_{13}	C_{33}	C_{44}	e_{31}	e_{33}	e_{15}	ε_{11r}	ε_{33r}
AlN	396	137	108	373	116	−0.58	1.55	−0.48	9	11
InN	223	115	92	224	48	−0.57	0.97	−0.22	15	15

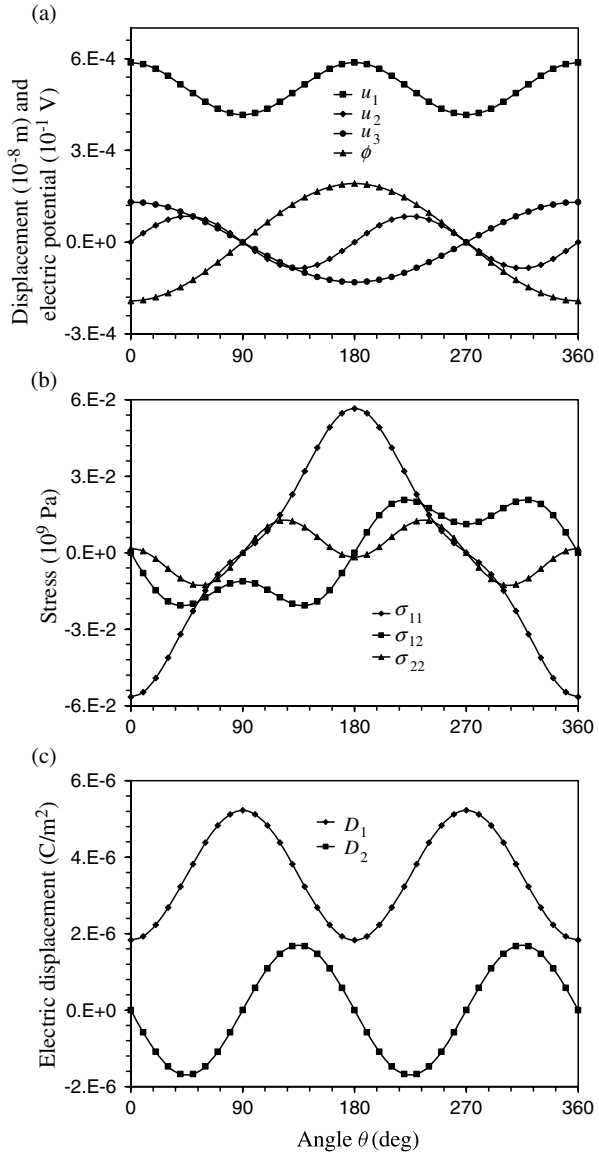

Figure 2. Variations of nonzero components of the piezoelectric field along a circle ($3h\cos\theta$, $3h\sin\theta$, 0) due to a surface point force applied along the x_1-axis at location (0, 0, 0).

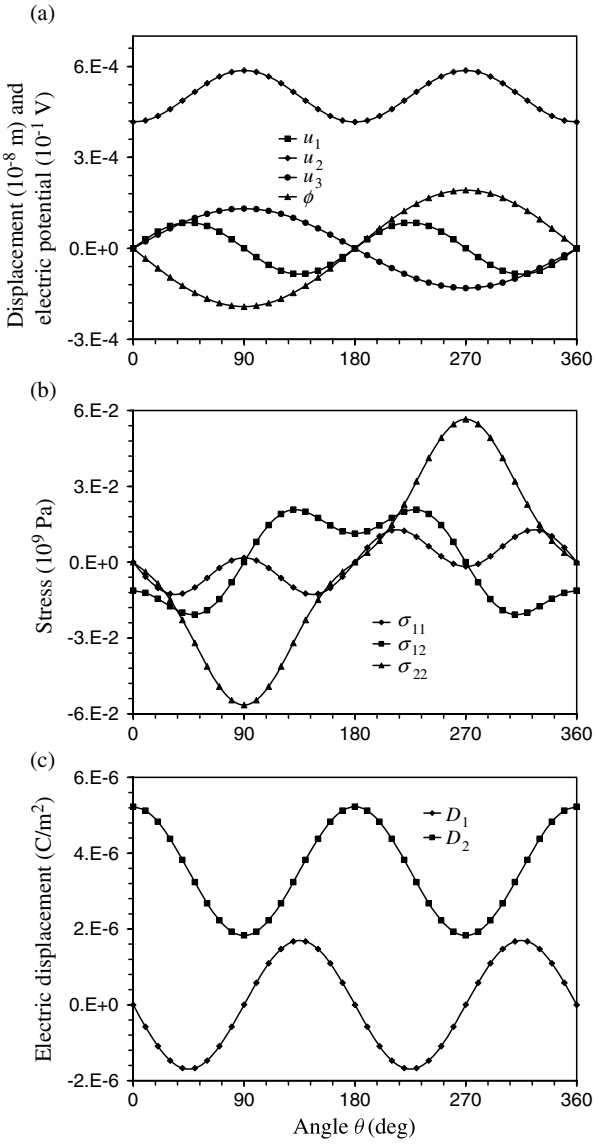

Figure 3. Variations of nonzero components of the piezoelectric field along a circle ($3h\cos\theta$, $3h\sin\theta$, 0) due to a surface point force applied along the x_2-axis at location (0, 0, 0).

The vertical variation of (nonzero) components of the piezoelectric field along the vertical line ($3h$, 0, x_3) is shown in figures 5–7. Because of the discontinuity of materials properties between adjacent layers, the vertical variation of the piezoelectric field through thickness in the structure is complicated. The elastic displacement, traction, electric potential, and normal component of electric displacement are continuous across the interfaces, consistent with the imposed interfacial conditions. However, these quantities exhibit kinks at the interfaces—their derivatives at the interfaces are discontinuous. In contrast, the in-plane components of stress and electric displacement exhibit jumps at the interfaces. There appears to be no simple pattern in these discontinuous variations, dictating that a full-field analysis is in general needed to understand the piezoelectric field in the layered AlN/InN structure subjected to a point force. Some of the piezoelectric components achieve a peak absolute value underneath the loading surface. For example, when the applied

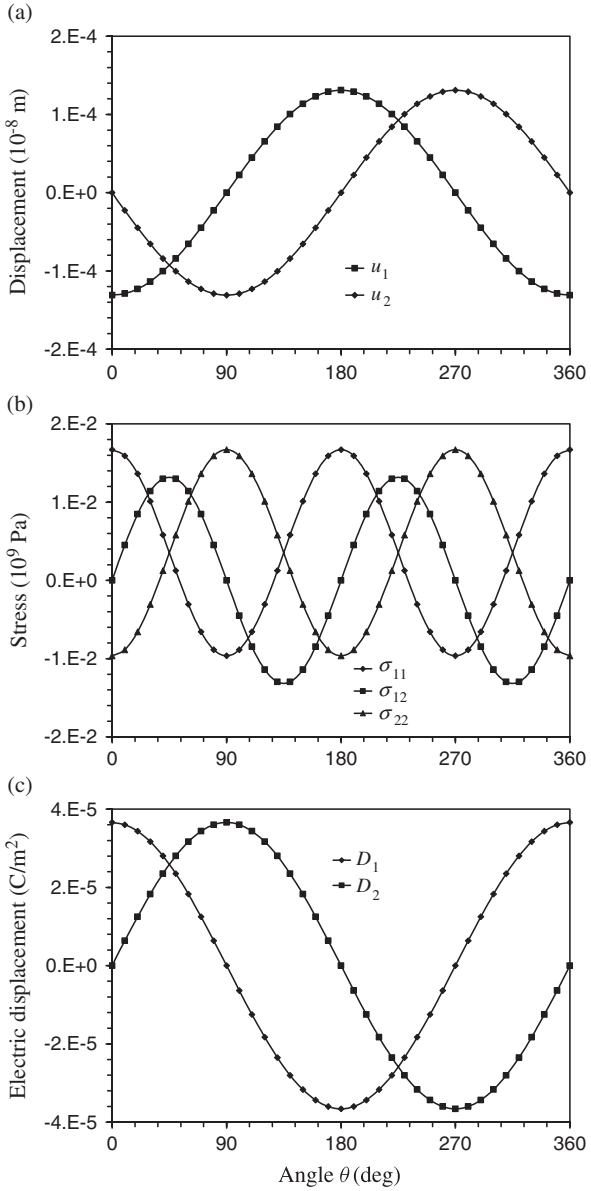

Figure 4. Variations of nonzero components of the piezoelectric field along a circle $(3h\cos\theta, 3h\sin\theta, 0)$ due to a surface point force applied along the x_3-axis at location (0, 0, 0). Nonzero components also include u_3 and ϕ, which are constant: $u_3 = 4.068 \times 10^{-12}$ m, $\phi = 1.067 \times 10^{-4}$ V.

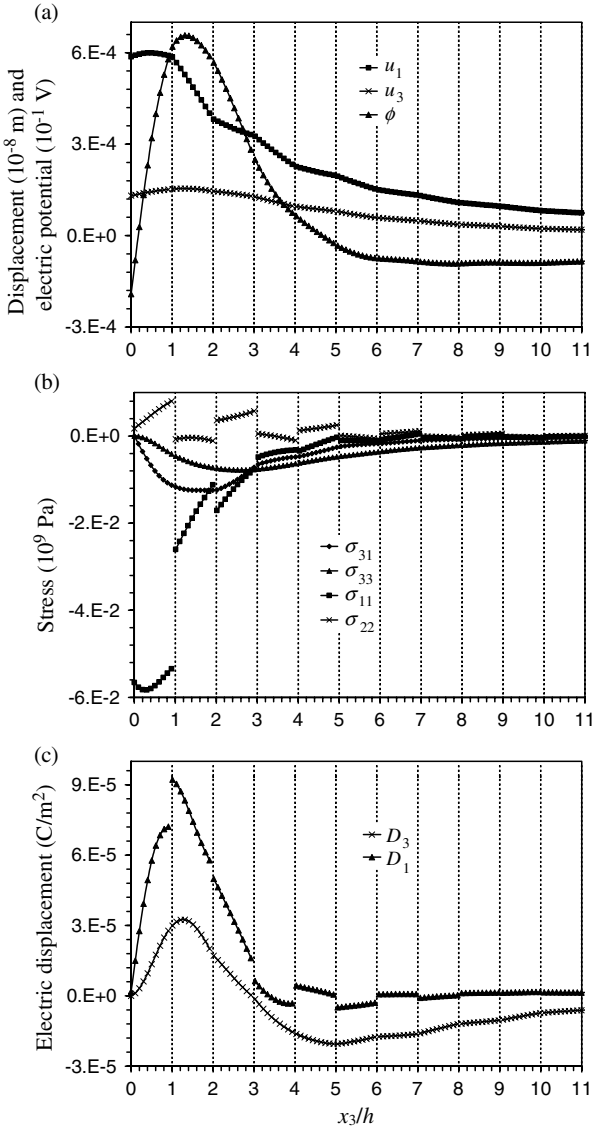

Figure 5. Variations of nonzero components of the piezoelectric field along a vertical line $(3h, 0, x_3)$ due to a surface point force applied along the x_1-axis at location (0, 0, 0).

point force is along the x_3-axis, a peak absolute value of D_1 occurs in the second layer underneath the loading surface, as shown in figure 7(c).

Finally, the radial variation of the piezoelectric field is examined to show the scaling behavior of the field. Figure 8 shows the radial variation of the nonzero components of the elastic displacement (times r), electric potential (times r), stress (times r^2), and electric displacement (times r^2) along the radial line $(r, 0, 0)$ due to a point force applied along the x_3-axis at (0, 0, 0). The dashed straight lines indicate the solutions in the case of homogeneous AlN half-space. The abscissa is plotted in the logarithmic scale. It can be seen that the piezoelectric responses in the layered structure due to the point force behave in the same asymptotic way as in the corresponding half-space case (Pan and Tonon 2000, Pan and Yuan 2000) in a very short distance from the point force, about one tenth of the layer thickness. Beyond that distance, the responses exhibit a significant influence of the layered heterogeneity. This holds true for the variations in all other radial directions. On the one hand, this study demonstrates the validity and accuracy of the present formulation. On the other hand, it shows the necessity of a 3D full-field analysis of the multilayered piezoelectric structure.

3.2. A point charge placed inside the layered structure

Now we consider the case where an interior point charge is applied to the layered structure. The point charge is placed at $(0, 0, 1.5h)$ in the middle plane of the second layer from the top. Its magnitude is equal to -10^{-16} C. The piezoelectric field along the horizontal line $(x_1, 0, 0)$ on the top surface is calculated, and the nonzero components are plotted in figure 9.

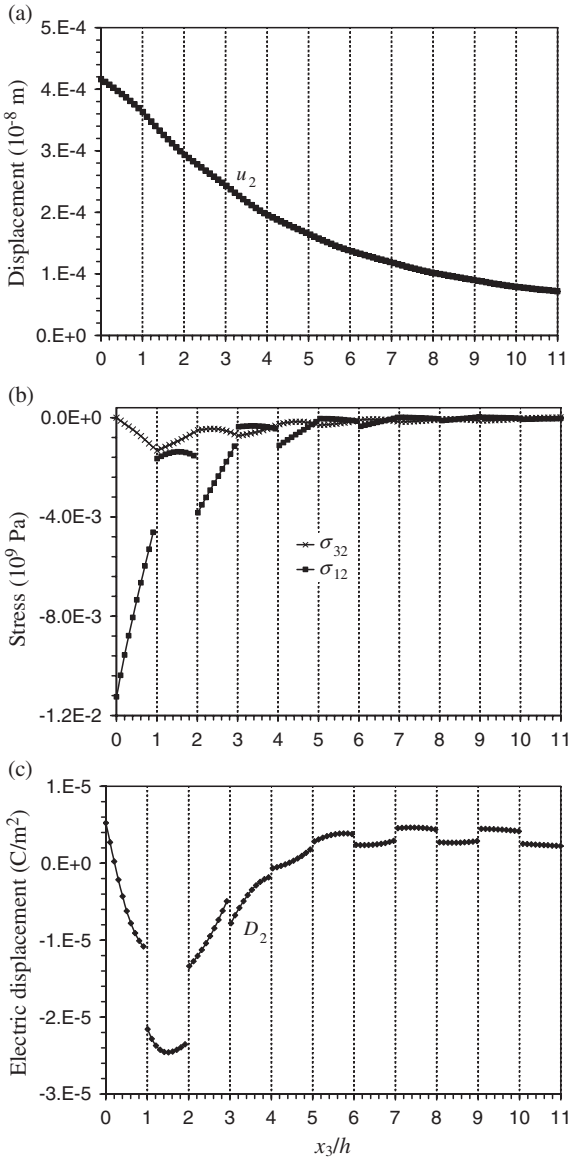

Figure 6. Variations of nonzero components of the piezoelectric field along a vertical line $(3h, 0, x_3)$ due to a surface point force applied along the x_2-axis at location (0, 0, 0).

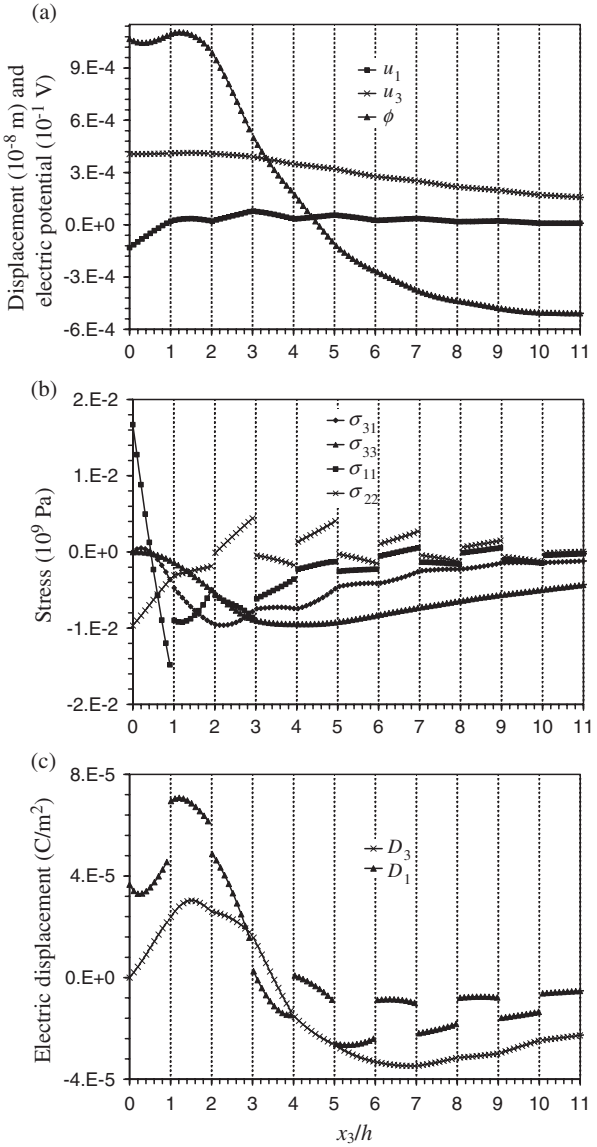

Figure 7. Variations of nonzero components of the piezoelectric field along a vertical line $(3h, 0, x_3)$ due to a surface point force applied along the x_3-axis at location (0, 0, 0).

Before discussing the numerical results, we mention that the response was also examined near the point charge. It was found that the response exhibits asymptotic behavior in the case of an infinite space of AlN in a very short distance, similar to that shown in figure 8.

The (negative) point charge induces a negative electric potential field on the top surface. The electric potential has the minimum value right above the point charge (figure 9(b)). The vertical elastic displacement u_3 induced by the point charge is negative when the observation point is close to the epicenter of the point charge, and becomes positive when the observation point is moved away from the epicenter to a distance of about h. The elastic displacement component u_3 is symmetric relative to the x_2-axis. The horizontal elastic displacement component u_1 is antisymmetric relative to the x_2-axis (figure 9(a)).

Corresponding to these elastic displacement and electric potential variations, the induced stress components, σ_{11} and σ_{22}, have a peak tensile value right above the point charge. Their magnitudes decrease when the observation point is moved away from the epicenter of the point charge. Furthermore, these stress components become compressive at a distance of about h from the epicenter. At large distances, all the stress components become trivial, i.e., the effect of the point charge is negligible (figure 9(b)). The electric displacement component, D_1, is antisymmetric relative to the x_1-axis. It is zero right above the point charge and trivial at large distance. It has a maximum value at about $x_1 = -h$, and a minimum value at about $x_1 = h$ (figure 9(c)).

4. Conclusions

Three-dimensional solutions in multilayered anisotropic piezoelectric structures subjected to a point force and/or a point charge have been derived within the framework of

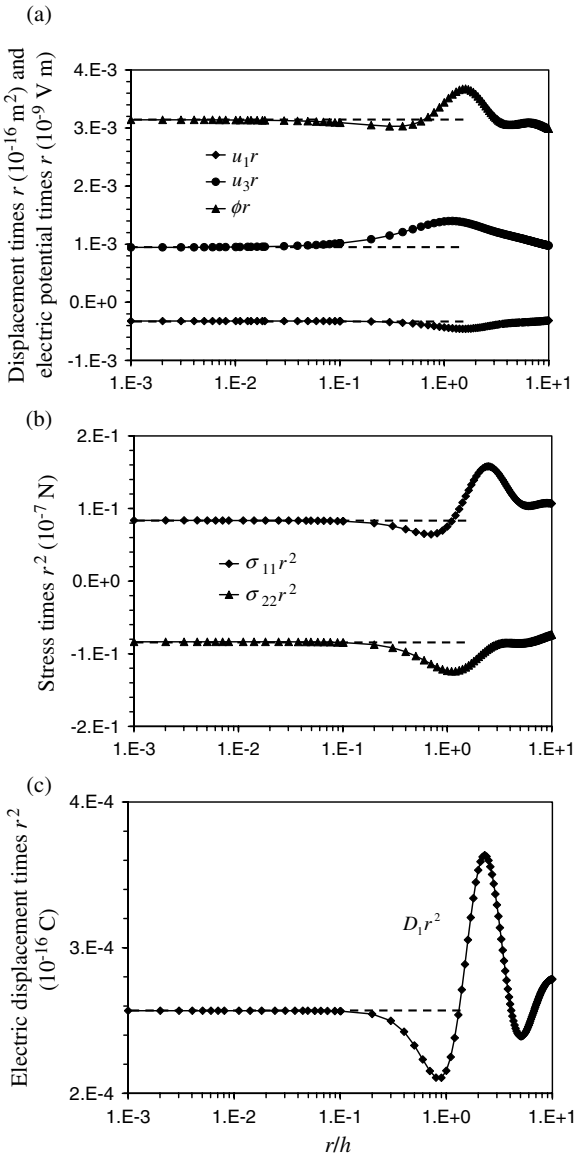

Figure 8. Variations of nonzero components of displacement times r, electric potential times r, stress times r^2, and electric displacement times r^2 along a horizontal line $(x_1, 0, 0)$ due to a surface point force applied along the x_3-axis at location (0, 0, 0), where $r = x_1$. The dashed lines indicate the solutions in the case of homogeneous AlN half-space.

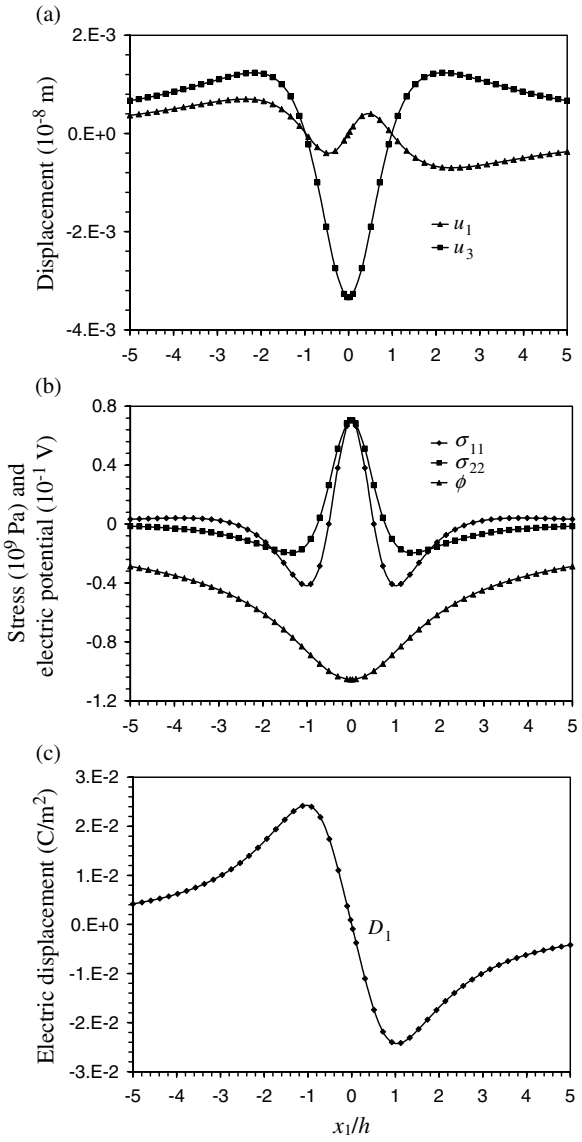

Figure 9. Variations of nonzero components of the piezoelectric field along a horizontal line $(x_1, 0, 0)$ due to a point charge placed at location $(0, 0, 1.5h)$ below the top surface.

the extended Stroh formalism and 2D Fourier transforms. The interfaces are perfectly bonded, where the continuity conditions of displacement, traction, electric potential, and normal component of electric displacement are imposed. General boundary conditions are considered at the top and bottom surfaces. These solutions are important to the investigation of practical smart composite laminates and semiconductor superlattices on various length scales.

Numerical results for a layered structure of ten alternating layers of piezoelectric AlN/InN on an AlN substrate are reported. Two cases are considered. In the first case, a point force is applied on the surface of the structure to simulate an indentation test. In the second case, a point charge is placed inside a layer to simulate the piezoelectric effect of a sink or source in the layered structure. The calculated piezoelectric fields satisfy the imposed boundary and interfacial conditions, which demonstrates the validity of the present formulation. Our numerical results show that the asymptotic behavior of the Green responses in the case of infinite space/half-space exists in a very short distance from the point source in the case of multilayered structures with surfaces and interfaces. The complicated patterns of the piezoelectric fields due to the layered heterogeneity with abrupt discontinuity demonstrate the necessity of a general 3D full-field analysis in the design of such smart structures.

Acknowledgments

BY is financially supported by Kent State University and Massachusetts Institute of Technology through the NSF project No 0121545.

References

Akamatsu M and Tanuma K 1997 Green function of anisotropic piezoelectricity *Proc. R. Soc.* A **453** 473–87

Barnett D M and Lothe J 1975 Dislocations and line charges in anisotropic piezoelectric insulators *Phys. Status Solidi* b **67** 105–11

Chen T 1993 Green functions and the non-uniform transformation problem in a piezoelectric medium *Mech. Res. Commun.* **20** 271–8

Chung M Y and Ting T C T 1996 Piezoelectric solid with an elliptic inclusion or hole *Int. J. Solids Struct.* **33** 3343–61

Davi G and Milazzo A 2002 Stress and electric fields in piezoelectric composite laminates *Electron. J. Bound. Elem.* **BETEQ 2001** 43–50

Deeg W F J 1980 The analysis of dislocation, crack, and inclusion problems in piezoelectric solids *PhD Dissertation* Stanford University, CA

Denda M and Lua J 1999 Development of the boundary element method for 2D piezoelectricity *Composites* B **30** 699–707

Ding H J, Chen B and Liang J 1997 On the Green functions for two-phase transversely isotropic piezoelectric media *Int. J. Solids Struct.* **34** 3041–57

Ding H J, Chi Y and Guo F 1999 Solutions for transversely isotropic piezoelectric infinite body, semi-finite body and bimaterial infinite body subjected to uniform ring loading and charge *Int. J. Solids Struct.* **36** 2613–31

Dunn M L and Wienecke H A 1996 Green functions for transversely isotropic piezoelectric solids *Int. J. Solids Struct.* **33** 4571–81

Dunn M L and Wienecke H A 1999 Half-space Green functions for transversely isotropic piezoelectric solids *J. Appl. Mech.* **66** 675–9

Jogai B 2001 Three-dimensional strain field calculations in multiple InN/AlN wurtzite quantum dots *J. Appl. Phys.* **90** 699–704

Liu Y J and Fan H 2001 On the conventional boundary integral equation formulation for piezoelectric solids with defects or of thin shapes *Eng. Anal. Bound. Elem.* **25** 77–91

Pan E 1999 A BEM analysis of fracture mechanics in 2D anisotropic piezoelectric solids *Eng. Anal. Bound. Elem.* **23** 67–76

Pan E 2001 Exact solution for simply supported and multilayered magneto-electro-elastic plates *J. Appl. Mech.* **68** 608–18

Pan E 2002 Mindlin's problem for an anisotropic piezoelectric half space with general boundary conditions *Proc. R. Soc.* A **458** 181–208

Pan E and Tonon F 2000 Three-dimensional Green functions in anisotropic piezoelectric solids *Int. J. Solids Struct.* **37** 943–58

Pan E and Yuan F G 2000 Three-dimensional Green functions in anisotropic piezoelectric bimaterials *Int. J. Eng. Sci.* **38** 1939–60

Ru C Q 2000 Eshelby's problem for two-dimensional piezoelectric inclusions of arbitrary shape *Proc. R. Soc.* A **456** 1051–68

Ru C Q 2001 Two-dimensional Eshelby problem for two bonded piezoelectric half-planes *Proc. R. Soc.* A **457** 865–83

Ting T C T 1996 *Anisotropic Elasticity* (Oxford: Oxford University Press)

Tzou H S 1993 *Piezoelectric Shells: Distributed Sensing and Control of Continua* (Norwell, MA: Kluwer–Academic)

Yang J S and Tiersten H F 1997 Elastic analysis of the transfer of shearing stress from partially electroded piezoelectric actuators to composite plates in cylindrical bending *Smart Mater. Struct.* **6** 333–40